Multiple Rabi Splittings under Ultrastrong Vibrational Coupling

Jino George,[1] Thibault Chervy,[1] Atef Shalabney,[1,2] Eloïse Devaux,[1] Hidefumi Hiura,[3] Cyriaque Genet,[1,*] and Thomas W. Ebbesen[1,†]

[1]*ISIS and icFRC, Université de Strasbourg and CNRS, 67000 Strasbourg, France*

[2]*Braude College, Snunit Street 51, Karmiel 2161002, Israel*

[3]*IoT Device Research Laboratories, NEC Corporation, 34 Miyukigaoka, Tsukuba 305-8501, Japan*

(Received 17 December 2015; revised manuscript received 9 June 2016; published 6 October 2016)

From the high vibrational dipolar strength offered by molecular liquids, we demonstrate that a molecular vibration can be ultrastrongly coupled to multiple IR cavity modes, with Rabi splittings reaching 24% of the vibration frequencies. As a proof of the ultrastrong coupling regime, our experimental data unambiguously reveal the contributions to the polaritonic dynamics coming from the antiresonant terms in the interaction energy and from the dipolar self-energy of the molecular vibrations themselves. In particular, we measure the opening of a genuine vibrational polaritonic band gap of ca. 60 meV. We also demonstrate that the multimode splitting effect defines a whole vibrational ladder of heavy polaritonic states perfectly resolved. These findings reveal the broad possibilities in the vibrational ultrastrong coupling regime which impact both the optical and the molecular properties of such coupled systems, in particular, in the context of mode-selective chemistry.

DOI: 10.1103/PhysRevLett.117.153601

Light-matter interactions in the strong coupling regime offer exciting possibilities for exploring quantum coherent effects from both a physical and a chemical perspective. This regime can be reached when a confined electromagnetic field interacts coherently with an electronic transition of an embedded material, leading to the formation of polaritonic states [1]. Many realizations of this effect have been demonstrated, ranging from single atoms [2], quantum wells [3,4], superconducting q bits [5] to molecular systems [6–13]. Recently, we demonstrated that molecular vibrations can be strongly coupled to an optical mode of a Fabry-Pérot (FP) cavity in the infrared (IR) region [14,15]. Such coupling is attracting more and more attention [16–18], since molecular vibrations play a key role in chemistry. Therefore, vibrational strong coupling could potentially be used to control chemical reactions in the same way as it has been demonstrated for electronic strong coupling [19]. Lately, a whole field of research has been opened with the prediction and demonstration of an ultrastrong coupling (USC) regime [20]. The USC regime indeed leads to the possibility of probing fascinating properties of the coupled states such as nonclassical ground-state behavior, squeezed vacuum, and polaritonic band gaps [21–25].

In this Letter, we demonstrate that USC can also be reached, at room temperature, with ground-state molecular vibrations coupled to an optical mode. Inherent features of the USC regime, antiresonant and self-energy contributions to the coupling, are measured on vibrational polaritonic states. These results reveal totally different dynamics than the one we previously reported for vibrational strong coupling [14]. To reach this vibrational USC regime, we exploit unique features of molecular liquids with a high vibrational dipolar strength. Such liquids resemble assemblies of individual ground-state mechanical oscillators where one is able to reach dipolar strength densities far beyond the quenching densities in the solid phase. These combined features naturally set the conditions for collective coupling strengths up to the USC regime. Remarkably, with Rabi splitting practically matching the free spectral range (FSR) of the IR cavity, the coupling process involves multiple orders of the FP cavity modes and leads to a genuine ladder of polaritonic states. We show multimode splitting with up to ten polaritonic peaks. The new vibrational spectrum associated with this polaritonic ladder differs radically from the vibrational spectrum of the bare molecules. While USC has been recognized as a new playground for electronic polaritonic physics, the USC features that we now observe on vibrations are expected to also have a strong impact on the chemistry of vibrational polaritonic states that remains so far unexplored.

Our system consists of a microfluidic FP flow cell which can be filled with any given molecular liquid (see Supplemental Material, Sec. A [26–32]). It is made of two ZnSe windows coated with 13 nm thick Au films to form the FP mirrors and closing them with a Mylar spacer of the appropriate thickness produces a microcavity with IR modes of quality factors $Q \sim 50$ [15]. By varying the spacer thickness, one of the optical modes is brought into resonance with the targeted molecular vibration. Different concentrations of molecules are injected in the cell, and the system is spectroscopically characterized using a commercial Fourier transform IR spectrophotometer (Nicolet-6700). The two molecules chosen for this study are the iron pentacarbonyl $Fe(CO)_5$ (see Fig. 1) and carbon

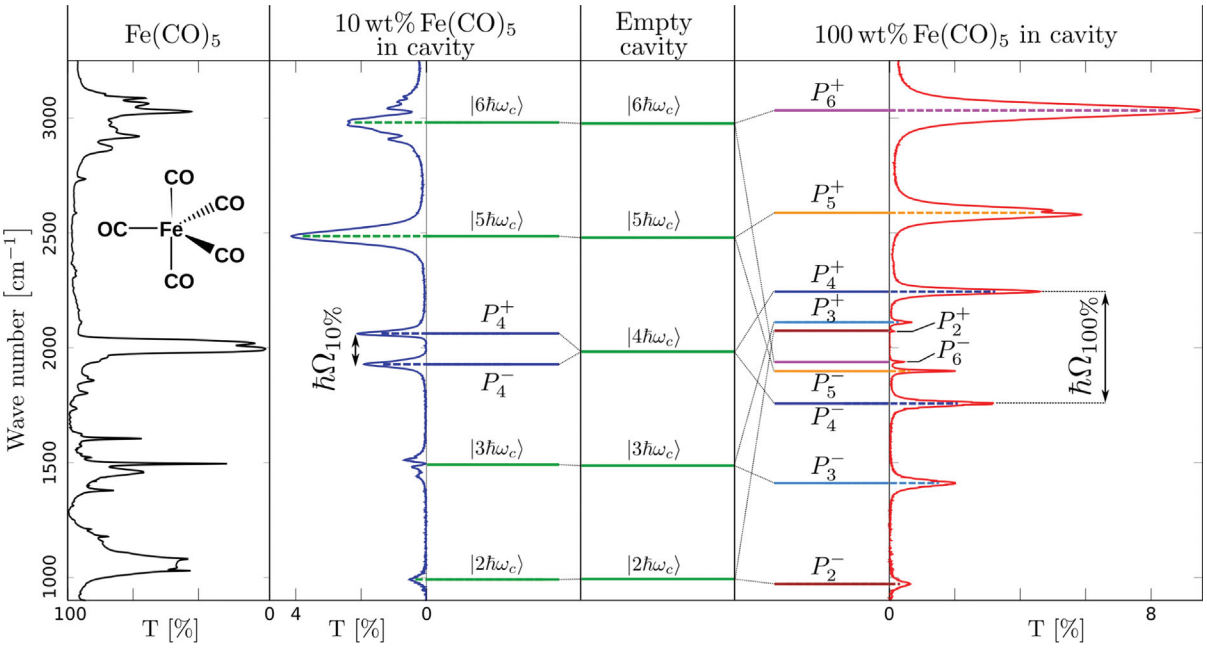

FIG. 1. $Fe(CO)_5$ data are shown in columns for clarity, starting with the IR spectrum of 10 wt. % $Fe(CO)_5$ in toluene, the transmission spectrum of the FP cavity filled with the same solution (blue curve) with a Rabi splitting $\Omega_{10\%} \sim 135$ cm^{-1}, followed by the mode diagram of the system under the corresponding coupling. The middle column shows the empty cavity modes with, on the right-hand side, the coupled diagram of the multiple polaritonic states when the cavity is filled with 100 wt. % $Fe(CO)_5$. The last column to the right shows the corresponding experimental IR spectrum of the filled cavity with a resonant Rabi splitting $\Omega_{100\%} \sim 480$ cm^{-1}.

disulphide CS_2. $Fe(CO)_5$ liquid has a very strong oscillator strength with three equatorial and two axial CO-stretching degenerate modes having a fundamental frequency ω_ν corresponding to a wave number of ~2000 cm^{-1} [33]. The IR absorption band of a dilute $Fe(CO)_5$ solution (10 wt. % in toluene) is shown in Fig. 1. We inject the same solution into a FP cavity tuned to have its fourth-order longitudinal mode resonant with the CO-stretching band. This resonant coupling splits the fundamental vibrational mode into an upper and lower mode separated by $\hbar\Omega_{10\%} \sim$ 135 cm^{-1} (Fig. 1, second column). Importantly, this mode splitting is larger than the width both of the cavity mode and of the vibrational peak; i.e., it corresponds to a genuine Rabi splitting.

Using pure $Fe(CO)_5$ liquid under the same resonant conditions expectedly leads to an increase in the mode splitting up to $\hbar\Omega_{100\%} \sim 480$ cm^{-1}, as shown in Fig. 1 (fourth column). In these conditions, the vibrational spectrum of the coupled $Fe(CO)_5$ liquid also displays a series of sharp resonances that stem from the coupling of the CO-stretching band with successive longitudinal modes of the FP cavity. We report in Supplemental Material (Sec. B [26]) similar spectral evolutions for CS_2. This multimode splitting theoretically predicted by Meiser and Meystre [34] is similar to that reported in the case of electronic strong coupling [35,36].

In order to understand the multipeaked structure of the spectrum, we perform a transfer matrix simulation on a cavity filled with pure $Fe(CO)_5$ liquid. Solving the multilayered structure consisting of the ZnSe flow cell windows, the Au cavity mirrors, and the embedded absorbing medium, the calculated cavity transmission spectrum is shown together with the measured spectrum in Fig. 2(a). A detailed description of the modeling of our system is given in Supplemental Material, Sec. A [26]. The electric field distribution inside the cavity was computed using the same parameters and is shown in Fig. 2(b). As can be seen from the field distributions, the CO-stretching mode of $Fe(CO)_5$, when resonantly coupled to the fourth-order mode of the FP cavity, gives rise to an upper and a lower mode, at 2245 and 1756 cm^{-1}, respectively. The other four new resonances on either sides of the fundamental CO-stretching mode are at 2110, 2071, 1938, and 1898 cm^{-1} (the other peaks outside this spectral window can be seen in Fig. 1). The field distributions enable us to identify the modes at higher energy as originating from the coupling between the vibrational band and lower optical modes of the cavity and vice versa for the modes at lower energy.

The positions of these modes is directly given by computing the round-trip phase accumulation $\delta\phi = 2L\omega n/c + 2\phi_r$ for the electromagnetic field in the cavity, where L is the cavity length, ω is the vacuum frequency of light, c is the speed of light, n is the real part of the refractive index, and ϕ_r is the reflection phase due to the finite metal skin depth [37]. As shown in Fig. 2(c), the dispersive character of the pure molecular liquid is so strong that optical modes of different mth orders can satisfy

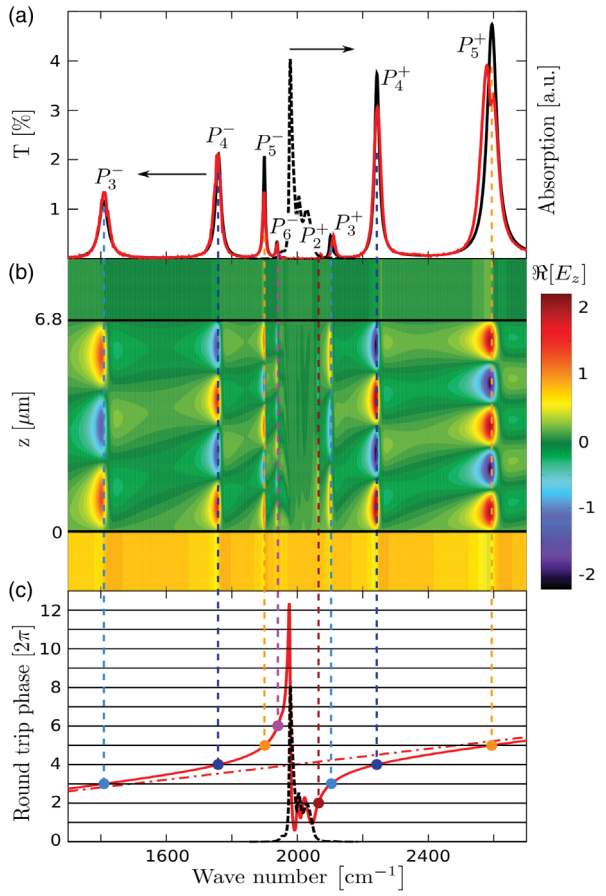

FIG. 2. (a) Experimental (red line) and transfer matrix simulated (black line) IR transmission spectra of pure $Fe(CO)_5$ coupled to the fourth-order mode of a flow cell FP cavity; black dashed line is the simulated absorbance of CO stretching mode of pure $Fe(CO)_5$. (b) T-matrix simulation of the electric field distribution inside the FP cavity. Asymmetric field distribution on either side of the vibrational band is an indication of higher and lower mode folding effects due to a strongly dispersive refractive index. (c) Round-trip phase accumulation of the electromagnetic field in the cavity with (red line) and without (red dashed line) an absorber. Optical resonances occur for phase accumulation equal to integer multiples of 2π (horizontal black lines). The dispersion of the refractive index of the intracavity medium allows multiple solutions for various mode indices (vertical dashed lines, the same color code as in Fig. 1). The fitted absorption line shape of $Fe(CO)_5$ is also shown in a black dashed line. The resonances lying in the strong absorption region are overdamped solutions and do not appear in the transmission spectra.

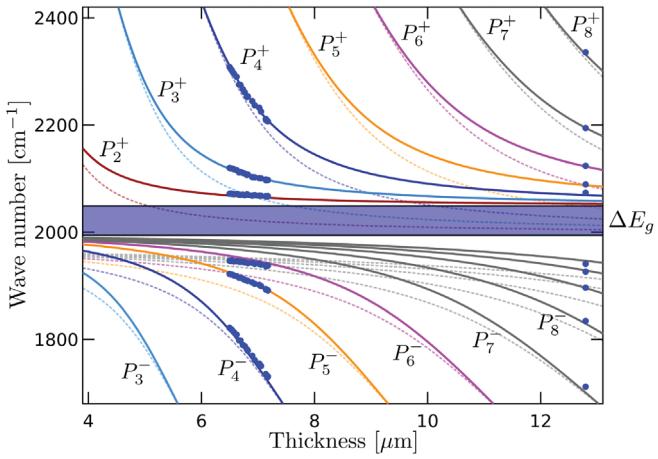

FIG. 3. Polaritonic dispersion diagram as a function of the cavity thickness. Experimental transmission peak positions are reported as blue dots. The exact cavity thickness is determined from the free spectral range of the cavity—see Supplemental Material (Sec. A [26]). The solid lines are the best fit to the data using the full Hamiltonian model that accounts for the dipolar self-energy and the contributions beyond the rotating wave approximation (RWA), while the dashed lines are solutions of the simple RWA model—see Supplemental Material (Sec. D [26]) for the fitting procedure. The color code is the same as in Fig. 1. The vibrational polaritonic band gap ΔE_g appears only in the full Hamiltonian model.

simultaneously the resonant phase condition $\delta\phi = 2\pi m$, with two solutions P_m^+, P_m^- for each mode m. The observed vibrational ladder is characterized by very large multimode splittings, with $\Omega_{100\%}$ reaching ca. 24% of the vibrational mode energy. Such a high ratio is often encountered in ultrastrongly coupled systems, and, in order to confirm that our molecular liquid has entered into the USC regime, we now show that the spectral structure of the coupled vibrational ladder cannot be described outside the framework of an ultrastrong light-matter interaction.

The involvement of specific features of the USC regime can be revealed most directly at the level of polaritonic dispersion diagrams. We have measured the dispersions of our coupled vibrational modes as a function of the cavity thickness (i.e., as a function of the detuning). This is done by varying the cavity thickness around a fixed value determined by the spacer inserted in our flow cell. The results are gathered in Fig. 3. Using a thicker spacer, we obtain the asymptotic positions of the coupled modes. These experimental data are compared to polaritonic dispersions that are calculated from a coupled oscillator model that takes explicitly into account the contributions of the vibrational dipolar self-energy in the molecular liquid and the antiresonant coupling terms which are specific to the USC regime (see Supplemental Material [26], Sec. C, for a detailed presentation of the model). We emphasize that, in our model, there is only one free parameter which corresponds to the Rabi splitting $\hbar\Omega_R$.

As discussed in Supplemental Material (Sec. D [26]), a coupled oscillator model keeping only the resonant interaction terms at $\mathcal{O}(\Omega_R/\omega_\nu)$ order, and therefore neglecting the dipolar self-energy of the vibration (Jaynes-Cummings-type Hamiltonian), is unable to fit accurately the experiment close to the bare vibrational mode energy, as shown in Fig. 3 (enlargement) and in full scale in Supplemental Material [26]. This mismatch proves that our system is truly

in the USC regime. Remarkably, the asymptotic values of the model yield a vibrational polaritonic band gap of $\sim 60\,\mathrm{cm}^{-1}$, as shown in Fig. 3. The opening of such a band gap is an indisputable signature of the USC regime, as pointed out in the context of intersubband electronic transition systems [23,24]. Here, we emphasize again that such a signature is observed for molecular vibrational transitions. More interestingly, the USC regime also implies that the vibrational ground state must shift to lower energies while acquiring a photonic admixture. Such modifications are analogous to those described at the level of electronic transitions, except that, in our case, they imply a deep modification of the whole vibronic landscape of the dressed molecules.

The second remarkable feature of the vibrational dressed states under USC is related to the presence of a genuine ladder of vibrational polaritonic states. To get further insight into the nature of these multiple polaritonic states, we perform angle-dependent experiments. The dispersion diagram shown in Fig. 4(a) clearly demonstrates the dispersive behavior of the different polaritonic states. This behavior is inherited from the photonic component of the polaritonic states and is the signature of their hybrid light-matter nature. Taking the Rabi frequency parameter extracted from the best fit of the polaritonic thickness-dependent dispersions of Fig. 3, our USC oscillator model perfectly matches these experimental angular dispersion data. Again, the polaritonic band gap is clearly seen, demonstrating that this forbidden energy band exists for any cavity thickness and at any angle. We stress that our model assumes no interaction between the polaritonic branches associated with different (orthogonal) cavity modes. However, nontrivial cross talk between the different polaritonic branches should be expected when accounting for the non-Markovian behavior of our system ($\Omega_{100\%} = 2k_BT$ [38]). This analysis, however, goes beyond the scope of this work. The results of our fit are shown in Fig. 4(a), and the extracted Hopfield coefficients for the polaritonic states P_4^- and P_6^- are shown in Fig. 4(b). As expected, the vibrational content of the states increases as they approach the energy of the bare vibrational mode. It is interesting to note the nontrivial evolution of the Hopfield coefficients calculated for the lower P_4^- polaritonic states which becomes more photonlike at resonance. This unbalanced matter- vs photonlike mixing fraction is another remarkable feature of the USC regime that comes in clear contrast with the usual regime of strong coupling. Between P_4^+ and P_4^-, the ladder consists of heavy (i.e., large vibrational content) polaritonic states. Surprisingly, those heavy polaritonic states display linewidths up to 5 times narrower than the width of the bare cavity mode and up to 6 times smaller than the linewidth of the bare (inhomogeneously broadened) molecular vibration. Because of the opening of the vibrational polaritonic band gap, these heavy polaritonic states are pushed away from the dissipative region of the bare vibration, therefore remaining perfectly resolved with their narrow linewidths. The concomitance of multimode and ultrastrong coupling of vibrational modes can hence be seen as an interesting way to overcome a major hurdle encountered in the physics of electronic strong coupling [39].

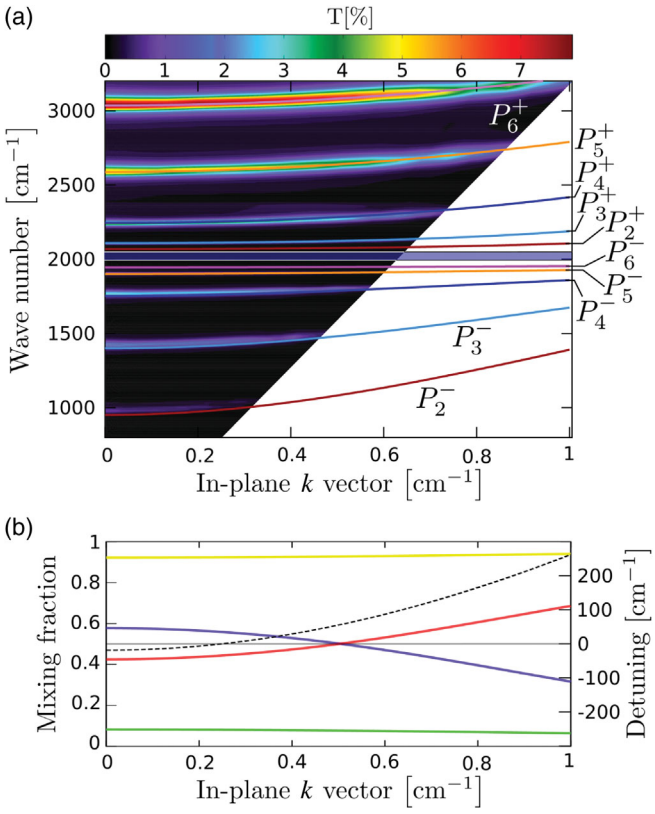

FIG. 4. (a) Polaritonic dispersion diagram measured by angle-dependent IR transmission spectroscopy (unpolarized, 0°–28°). The solid lines are the solutions of the full Hamiltonian model, using the same parameters and color code as in Fig. 3. The vibrational polaritonic band gap is again clearly observed (blue horizontal band). (b) Photonic and vibrational fractions of the P_4^- polaritonic branch (blue and red curves, respectively) and of the P_6^- polaritonic branch (green and yellow curves, respectively). The photon-vibration energy detuning for the fourth cavity mode is shown in black dashes (right axis).

In summary, we have demonstrated that it is possible to reach the regime of USC in the vibrational realm. This is done using high oscillator strength molecular liquids. We have revealed indisputable signatures of the USC regime, showing how the features inherent to the USC regime can be also found at the level of molecular vibrational modes. Remarkably, the molecular polaritonic multimode folding shown here is a practical way for generating heavy polaritonic states with smaller linewidths than both the optical transition and the molecular vibration, leading to an enhanced coherence time [40]. Perhaps more importantly, these results point to the potential impact of the USC regime in the context of bond-selective chemistry. As we already proposed [14,19], the dynamics of bond breaking in

the ground state could be significantly modified by vibrational strong coupling and even more under the USC regime where the whole vibrational ladder dressed by the IR cavity field is redefined. All these features will no doubt impact the optical, the molecular, and the material properties of these ultrastrongly coupled systems [41], enriching the possibilities offered by such light-matter interactions.

We thank David Hagenmüller for fruitful discussions. This work was supported in part by the European Research Council (Grant No. 22577), the Agence Nationale de la Recherche (ANR) Equipex 'Union' (ANR-10-EQPX-52-01), the Labex 'Nanostructures in Interaction with their Environment' (NIE) Projects (ANR-11-LABX-0058-NIE), and the University of Strasbourg Institute of Advanced Studies (USIAS) within the Investissement d'Avenir program (ANR-10-IDEX-0002-02).

J. G. and T. C. contributed equally to this work.

*Corresponding author.
genet@unistra.fr
†Corresponding author.
ebbesen@unistra.fr

[1] V. M. Agranovich, Y. N. Gartstein, and M. Litinskaya, Chem. Rev. **111**, 5179 (2011).
[2] J. M. Raimond, M. Brune, and S. Haroche, Rev. Mod. Phys. **73**, 565 (2001).
[3] M. S. Skolnick, T. A. Fisher, and D. M. Whittaker, Semicond. Sci. Technol. **13**, 645 (1998).
[4] E. Peter, P. Senellart, D. Martrou, A. Lemaitre, J. Hours, J. M. Gérard, and J. Bloch, Phys. Rev. Lett. **95**, 067401 (2005).
[5] A. Wallraff, D. I. Schuster, A. Blais, L. Frunzio, R.-S. Huang, J. Majer, S. Kumar, S. M. Girvin, and R. J. Schoelkopf, Nature (London) **431**, 162 (2004).
[6] I. Pockrand, A. Brillante, and D. Möbius, J. Chem. Phys. **77**, 6289 (1982).
[7] D. G. Lidzey, D. D. C. Bradley, M. S. Skolnick, T. Virgili, S. Walker, and D. M. Whittaker, Nature (London) **395**, 53 (1998).
[8] R. J. Holmes and S. R. Forrest, Phys. Rev. Lett. **93**, 186404 (2004).
[9] J. Bellessa, C. Bonnand, J. C. Plenet, and J. Mugnier, Phys. Rev. Lett. **93**, 036404 (2004).
[10] J. Dintinger, S. Klein, F. Bustos, W. L. Barnes, and T. W. Ebbesen, Phys. Rev. B **71**, 035424 (2005).
[11] J. D. Plumhof, T. Stäferle, L. Mai, U. Scherf, and R. F. Mahrt, Nat. Mater. **13**, 247 (2014).
[12] E. Orgiu, J. George, J. A. Hutchison, E. Devaux, J. F. Dayen, B. Doudin, F. Stellacci, C. Genet, J. Schachenmayer, C. Genes, G. Pupillo, P. Samori, and T. W. Ebbesen, Nat. Mater. **14**, 1123 (2015).
[13] P. Törmä and W. L. Barnes, Rep. Prog. Phys. **78**, 013901 (2015).
[14] A. Shalabney, J. George, J. Hutchison, G. Pupillo, C. Genet, and T. W. Ebbesen, Nat. Commun. **6**, 5981 (2015).
[15] J. George, A. Shalabney, J. A. Hutchison, C. Genet, and T. W. Ebbesen, J. Phys. Chem. Lett. **6**, 1027 (2015).
[16] M. Muallem, A. Palatnik, G. D. Nessim, and Y. R. Tischler, Ann. Phys. (Amsterdam) **528**, 313 (2015).
[17] J. P. Long and B. S. Simpkins, ACS Photonics **2**, 130 (2015).
[18] J. del Pino, J. Feist, and F. J. Garcia-Vidal, New J. Phys. **17**, 053040 (2015).
[19] J. A. Hutchison, T. Schwartz, C. Genet, E. Devaux, and T. W. Ebbesen, Angew. Chem., Int. Ed. **51**, 1592 (2012).
[20] C. Ciuti, G. Bastard, and I. Carusotto, Phys. Rev. B **72**, 115303 (2005).
[21] Y. Todorov, A. M. Andrews, R. Colombelli, S. De Liberato, C. Ciuti, P. Klang, G. Strasser, and C. Sirtori, Phys. Rev. Lett. **105**, 196402 (2010).
[22] G. Scalari, C. Maissen, D. Turčinková, D. Hagenmüller, S. De Liberato, C. Ciuti, C. Reichl, D. Schuh, W. Wegscheider, M. Beck, and J. Faist, Science **335**, 1323 (2012).
[23] B. Askenazi, A. Vasanelli, A. Delteil, Y. Todorov, L. Andreani, G. Beaudoin, I. Sagnes, and C. Sirtori, New J. Phys. **16**, 043029 (2014).
[24] S. Gambino, M. Mazzeo, A. Genco, O. Di Stefano, S. Savasta, S. Patanè, D. Ballarini, F. Mangione, G. Lerario, D. Sanvitto, and G. Gigli, ACS Photonics **1**, 1042 (2014).
[25] T. Schwartz, J. A. Hutchison, C. Genet, and T. W. Ebbesen, Phys. Rev. Lett. **106**, 196405 (2011).
[26] See Supplemental Material at http://link.aps.org/supplemental/10.1103/PhysRevLett.117.153601 for detailed descriptions of the T-matrix simulations, the CS_2 experimental results, the model for ultrastrongly coupled vibrational oscillators, and the dispersion data fitting procedure, which includes Refs. [27–32].
[27] A. D. Rakić, A. B. Djurišić, J. M. Elazar, and M. L. Majewski, Appl. Opt. **37**, 5271 (1998).
[28] E. K. Plyler and C. J. Humphreys, J. Res. Natl. Bur. Stand. **39**, 59 (1947).
[29] B. N. Figgis, Compr. Coord. Chem. **1**, 213 (1987).
[30] C. Cohen-Tannoudji, J. Dupont-Roc, and G. Grynberg, *Photons and Atoms: Introduction to Quantum Electrodynamics* (Wiley-VCH, New York, 1997).
[31] J. Hopfield, Phys. Rev. **112**, 1555 (1958).
[32] S. G. Johnson, http://ab-initio.mit.edu/nlopt.
[33] R. Cataliotti, A. Foffani, and L. Marchetti, Inorg. Chem. **10**, 1594 (1971).
[34] D. Meiser and P. Meystre, Phys. Rev. A **74**, 065801 (2006).
[35] E. Dupont, J. A. Gupta, and H. C. Liu, Phys. Rev. B **75**, 205325 (2007).
[36] X. Yu, D. Xiong, H. Chen, P. Wang, M. Xiao, and J. Zhang, Phys. Rev. A **79**, 061803 (2009).
[37] Y. Zhu, D. J. Gauthier, S. E. Morin, Q. Wu, H. J. Carmichael, and T. W. Mossberg, Phys. Rev. Lett. **64**, 2499 (1990).
[38] A. Canaguier-Durand, C. Genet, A. Lambrecht, T. W. Ebbesen, and S. Reynaud, Eur. Phys. J. D **69**, 24 (2015).
[39] A. Trichet, E. Durupt, F. Médard, S. Datta, A. Minguzzi, and M. Richard, Phys. Rev. B **88**, 121407 (2013).
[40] D. O. Krimer, B. Hartl, and S. Rotter, Phys. Rev. Lett. **115**, 033601 (2015).
[41] J. Galego, F. J. Garcia-Vidal, and J. Feist, Phys. Rev. X **5**, 041022 (2015).